Automatic cloud amount detection by surface longwave downward radiation measurements

Bruno Dürr and R. Philipona

Physikalisch-Meteorologisches Observatorium and World Radiation Center Davos, Davos-Dorf, Switzerland

Received 25 September 2003; revised 14 January 2004; accepted 22 January 2004; published 3 March 2004.

[1] Naked-eye observation of sky cloud cover has widely resisted automation. Automatic cloud cover detection systems suitable also for nighttime operation often demand large equipment investments and expensive data processing. An automatic partial cloud amount detection algorithm (APCADA) is presented, based only on accurate measurements of longwave downward radiation, temperature, and relative humidity at screen level height. APCADA provides cloud cover estimates every 10 min during daytime and nighttime and is applicable to radiation stations without knowledge of synoptic cloud observations. Naked-eye observations from seven radiation sites spanning from arctic to tropical climates have been compared to APCADA estimates. Results show that about 86% of all cases agree within ±1-octa cloud amount difference for sites with moderate climate, 82% for sites with arctic climate, and 78% for the site with tropical climate. For a maximum ±2-octa cloud amount difference, average site percentages range from 90% up to 95%. *INDEX TERMS:* 1640 Global Change: Remote sensing; 3394 Meteorology and Atmospheric Dynamics: Instruments and techniques; 3360 Meteorology and Atmospheric Dynamics: Remote sensing; 3359 Meteorology and Atmospheric Dynamics: Radiative processes; *KEYWORDS:* automatic cloud detection, longwave radiation, APCADA

Citation: Dürr, B., and R. Philipona (2004), Automatic cloud amount detection by surface longwave downward radiation measurements, *J. Geophys. Res.*, *109*, D05201, doi:10.1029/2003JD004182.

1. Introduction

[2] Synoptic observer reports are still the main source for cloud cover information at the surface worldwide. An increasing number of airports, however, are nowadays equipped with automated surface observation systems (ASOS), where cloud height and sky cloud cover are assessed by a ceilometer [*Nadolski*, 1995]. Ceilometers have the major disadvantage that they are often operated in a fixed direction only. Further efforts have been undertaken to improve ceilometer-based cloud cover estimations with longwave downward radiation measurements and usage of a neural network [*Aviolat et al.*, 1998]. An automatic cloud cover detection method based on IR pyrometers (8–14 μm) scanning the whole sky within 30 s was proposed by *Gillotay et al.* [2002]. Hemispheric sky imagers [*Long and DeLuisi*, 1998; *Beaubien and Bisberg*, 1999; *Feister et al.*, 2000] have the disadvantage of high equipment investment and extensive data processing. Sky imager systems and other cloud detection methods based on shortwave flux modification by the presence of clouds [*Long and Ackermann*, 2000] are available only for daytime observations.

[3] In this paper, the automatic partial cloud amount detection algorithm (APCADA) is introduced, which provides a simple and robust real-time cloud detection method available 24 hours a day. APCADA is based on an enhanced version of the clear-sky index (CSI) [*Marty and Philipona*, 2000], which is primarily used to extract cloud-free situations for radiative climate research. Long-term series of longwave downward radiation measurements from the Alpine Surface Radiation Budget (ASRB) network [*Philipona et al.*, 1996; *Marty et al.*, 2002] and from the Baseline Surface Radiation Network (BSRN) [*Ohmura et al.*, 1998] provided an extensive data set to implement and verify APCADA for different climate zones.

0148-0227/04/2003JD004182$09.00

2. Observational Data

2.1. ASRB Network

[4] The ASRB network consists of 10 stations between 370 and 3580 m above mean sea level (MSL) in the Swiss Alps (status end of 2002). Broadband and hemispherically integrated longwave downward radiation (LDR) and shortwave global radiation are measured. In collaboration between the Physikalisch-Meteorologisches Observatorium Davos/World Radiation Center (PMOD/WRC) and the Federal Office of Meteorology and Climatology (MeteoSwiss) the ASRB network was built at locations of the MeteoSwiss automatic network in 1994/95.

[5] Eppley Precision Infrared Radiometer (PIR) pyrgeometers are used to measure LDR at screen level height, i.e., 2 m above the surface. PIR outputs are sampled every 2 s and averaged over 2 min. The PIRs were modified at PMOD/WRC to improve uncertainty to ±3 W m^{-2} [*Philipona et al.*, 1995]. An extended round-robin experiment revealed that PIR measurements remained stable over a long time period [*Philipona et al.*, 1998]. The ASRB

instruments are calibrated in situ against a traveling standard every 3 years. Ten-minute averages of LDR measurements were used for investigations presented in this paper.

[6] ASRB instruments are artificially ventilated with a slightly heated airstream to protect the instrument domes from snow and ice coverage and to reduce the cloud-free temperature gradient between the instrument's body and dome [*Marty et al.*, 2002]. The remoteness of the stations and harsh weather conditions did not allow us to use a common mechanical shading disc system for the PIRs. Instead, all sites are equipped with a fixed shadow band in direction south. The dip of LDR due to the shadow at solar noon is used to correct the inadvertent shortwave influence on the LDR measurement [*Marty*, 2000].

[7] All ASRB sites are equipped with the ventilated thermohygrometer VTP6 [*Ruppert*, 1991]. The VTP6 measures air temperature and relative humidity at screen level height. Instantaneous values are obtained every 10 min averaged over 40 s. VTP6 functions well also under very cold and stormy alpine weather conditions. For this paper, 10-min averages of temperature and water vapor pressure were applied.

2.2. BSRN Network

[8] The BSRN consists of about 30 radiation sites worldwide. LDR measurements with a modified PIR were available from Ny Ålesund on Spitzbergen. However, Kwajalein, located on the Marshall Islands, operates an original PIR. The uncertainty of this PIR is on the order of ±5 W m^{-2} [*Philipona et al.*, 2001]. LDR, temperature, and relative humidity measurements are measured every minute, but values averaged over 10 min were applied only. Information about all stations used in this paper is given in Table 1.

2.3. Synoptic Observations

[9] At the ASRB sites PAY, LOM, and JFJ, synoptic observations are taken every 3 hours, but only from 0600 UTC to 1800 UTC at LOM and JFJ. At DAV and WFJ, simplified synoptic observations including total cloud amount and estimations of the optical density of clouds are made every 6 hours from 0600 to 1800 UTC.

[10] Synoptic observations are obtained every 6 hours at the BSRN locations KWA and NYA, except midnight (0000 UTC) at NYA. Information about total cloud cover, partial cloud cover, and cloud type was used.

[11] The exact synoptic observation time used in Switzerland is 30 to 40 min earlier than the official synoptic time, e.g., from 1120 to 1130 UTC for the 1200 UTC observation. Therefore observations were compared with an APCADA estimated partial cloud amount based on 10-min averages of LDR, temperature, and humidity from 1120 to 1130 UTC. Synoptic observations are taken 10 min later in NYA and 30 min later in KWA.

[12] Nighttime synoptic observations are used only if Moon elevation is higher than 10 degrees and Sun elevation is higher than −9 degrees, and Moon phase is at least half Moon at the same time. This guarantees acceptable light conditions for the observer [*Hahn et al.*, 1995].

3. Limitations on Total Cloud Amount Detection

[13] For cloud-free situations, about 60% of measured LDR stems from the first 100 m, and about 90% stems from the first 1000 m air column above the surface [*Ohmura*, 2001]. Hence high clouds (cirrus, cirrostratus, and cirrocumulus) are expected to produce a small effect on LDR at the Earth's surface because of large distance and cold emittance temperature. The influence of cirrus clouds on LDR in Payerne was investigated with the radiative transfer model MODTRAN v4.0 [*Berk et al.*, 2000] using MODTRAN cirrus cloud model number 18 and cloud-free radiosonde profiles measured in Payerne. The cirrus layer in the model covered the whole sky with an extinction coefficient equal to 0.14 km^{-1} at 0.55 micron, 1-km layer thickness, and cloud base at 6 km above MSL. The modeled hemispherically integrated effect on LDR was 4 W m^{-2} for summer and 5 W m^{-2} for winter radiosonde profiles. Hence LDR measured at the Earth's surface is marginally affected by high clouds, and therefore only total cloud amounts without high clouds (hereinafter referred to as partial cloud amount (PCA)) were further investigated. PCA is not directly observed and has to be calculated from other synoptic quantities. Such a calculation can be done using information like cloud type (C_L, C_M, and C_H for low, middle, and high clouds, respectively), total cloud amount (N), and partial cloud cover (N_h). N_h is defined as the cloud amount of C_L or, if no C_L clouds are present, of C_M clouds. Cloud type equal to zero means that no clouds were observed on the corresponding level. As an example, PCA is determined from the following observations in Payerne at 1200 UTC on 6 April 1999: N = 3 octas (1 octa means one-eighth of visible sky surface covered by clouds), $N_h = 2$, $C_L = 0$, $C_M = 3$, and $C_H = 2$. $N_h = 2$ corresponds directly to the amount of C_M clouds, because C_L clouds are missing. Thus PCA is equal to N_h, i.e., 2 octas. However, PCA could not be determined for some cases with three different cloud layers. A respective example was observed 3 hours later at 1500 UTC: $N = 5$, $N_h = 1$, $C_L = 5$, $C_M = 4$, and $C_H = 2$. The amount of C_L clouds is known ($N_h = 1$), but the rest of the $N - N_h = 4$ octas cloud amount cannot be clearly separated into the two remaining cloud layers (C_M and C_H). Thus PCA remains undefined for this case. PCA could be clearly deduced from synoptic observations for about 90% of all daytime (1200 UTC) and for more than 95% of all nighttime (0000 UTC) cases at all sites except KWA, where only about 40% of all possible PCA cases could be calculated.

4. Automatic Partial Cloud Amount Detection

4.1. Variability of Longwave Downward Radiation

[14] LDR measured at the surface over a period of 1 hour is strongly influenced by passing broken clouds. However, cloud-free and totally overcast situations, e.g., fog, are characterized by small LDR variations. To measure LDR variability, measurements over the last hour (60 min) are linearly interpolated, and the standard deviation of the residuals to the linear regression (Stdev LDR) is calculated. The comparison of Stdev LDR with observed PCA in Payerne shown in Figure 1a indicates that LDR variability is useful to separate broken cloud from cloud-free or overcast situations.

4.2. Enhanced Clear-Sky Index

[15] The clear-sky index (CSI) [*Marty and Philipona*, 2000] is intended to separate cloudy sky from cloud-free

Table 1. Radiation Stations, Short Name, Radiation Network, Altitude, Coordinates, and Data Set Used

Station	Abbreviation	Type	Altitude	Coordinates	Data Set
Kwajalein	KWA	BSRN	10 m	8°43′N, 167°44′E	2000–2001
Ny Ålesund	NYA	BSRN	42 m	78°56′N, 11°57′E	1999–2001
Locarno-Monti	LOM	ASRB	370 m	46°10′N, 8°47′E	1996–2002
Payerne	PAY	ASRB	490 m	46°49′N, 6°57′E	1996–2002
Davos	DAV	ASRB	1610 m	46°49′N, 9°51′E	1996–2002
Weissfluhjoch	WFJ	ASRB	2690 m	46°50′N, 9°49′E	1996–2002
Jungfraujoch	JFJ	ASRB	3580 m	46°33′N, 7°59′E	1996–2002

situations on the basis of LDR, screen level temperature, and water vapor pressure at the Earth's surface. The CSI is defined as

$$CSI = \frac{\epsilon_A}{\epsilon_{AC}}, \tag{1}$$

$$\epsilon_A = \frac{LDR}{\sigma_b T^4}, \tag{2}$$

$$\epsilon_{AC} = \epsilon_{AD} + (k + 2\sigma)\left(\frac{e}{T}\right)^{1/8}, \tag{3}$$

where σ_b is the Stephan-Boltzmann constant, T is the air temperature (K), ϵ_{AD} is an altitude-dependent emittance of a completely dry atmosphere, e is water vapor pressure (Pa), and k is a constant location-dependent coefficient. Water vapor pressure e is calculated from the relative humidity using the following equations:

$$e = \frac{RH}{100} e_s, \tag{4}$$

$$e_s = 6.1121 \exp\left(\frac{17.502 t_a}{t_a + 240.97}\right). \tag{5}$$

The empirical equation for the saturated water vapor pressure e_s (in hPa) is valid from −30°C to 50°C [*Buck*, 1981]. The air temperature t_a has to be in °C. Coefficient k is fitted to a set of manually selected cloud-free cases. The corresponding confidence level 2σ is added to k in order to include most of the cloud-free situations. The ϵ_A indicates the apparent emittance of the sky, and ϵ_{AC} indicates an empirical apparent cloud-free emittance. CSI $\leq$ 1 means cloud-free conditions, and CSI > 1 means cloudy sky [*Marty and Philipona*, 2000]. Comparisons with synoptic observations revealed that the application of CSI during nighttime underestimates the number of cloud-free situations. Further investigations of cloud-free cases with Payerne radiosonde data showed that high CSI values are correlated ($r \approx 0.6$) with negative vertical temperature gradients γ, i.e., temperature inversions, near the surface during nighttime and daytime. Here, γ is defined as $\gamma = (-(\Delta T/\Delta z))$, where ΔT is the temperature difference over a vertical distance $\Delta z \approx 30$ m. Thus variations of γ with time ($\gamma(t)$) have to be considered for the calculation of CSI. However, very few radiation sites regularly measure $\gamma(t)$. Further investigations showed that diurnal and annual cycle of $\gamma(t)$ can be roughly approximated as a periodical function:

$$\gamma(t) = \gamma_0 + \gamma_{amp} \cos\left(\omega t - \frac{\pi}{4}\right), \tag{6}$$

with γ_0 the average and γ_{amp} the amplitude of γ and $\omega = 2\pi/P$ with period $P = 1$ year or $P = 1$ day. The maximum of $\gamma(t)$ lags behind maximum solar insolation with approximately $\pi/4$ phase shift, i.e., 3 hours and 1.5 months for the diurnal and annual cycles, respectively. Thus we defined k in equation (3) as a function of $\gamma(t)$ and accordingly replaced k by $k = k[\gamma(t)] = k(t)$:

$$k(t) = k_0 + k_{amp} \cos\left(\omega t - \frac{\pi}{4}\right), \tag{7}$$

with $k_0 = (k_{max} - k_{min})/2$ and $k_{amp} = k_{max} - k_0$. Analogously, the constant confidence level 2σ in equation (3)

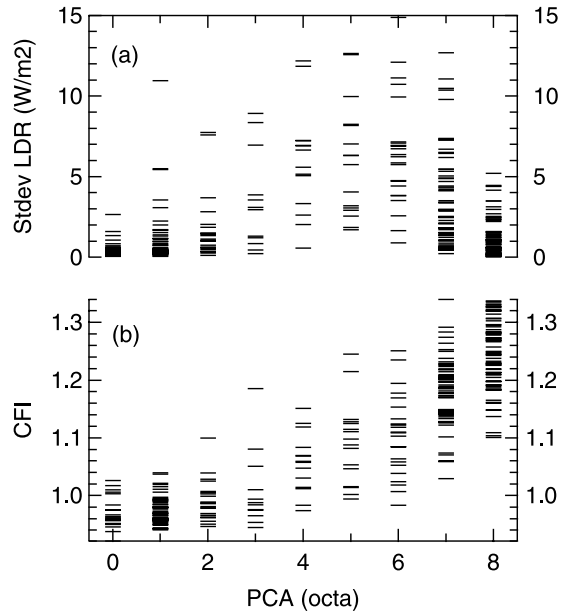

Figure 1. (a) Variability of longwave downward radiation within the last hour (Stdev LDR) and (b) cloud-free index (CFI) plotted against partial cloud amount (PCA) for 322 daytime observations (1200 UTC) in Payerne in 2001. CFI allows one to separate cloud-free (0- or 1-octa) and overcast (7- or 8-octa) situations. Compared to cloud-free or overcast conditions, broken cloud amounts (2–6-octa) are both characterized by different CFI values and large LDR variability.

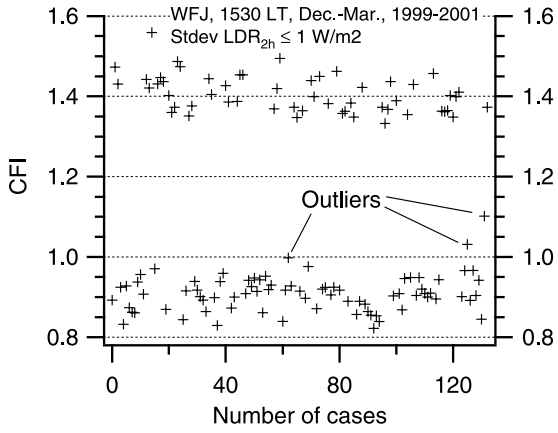

Figure 2. Calculated cloud-free index (CFI) values plotted for daytime (1530 LT) winter.

was replaced with a time-dependent shift function $\Delta k(t)$:

$$\Delta k(t) = \Delta k_0 + \Delta k_{\text{amp}} \cos\left(\omega t - \frac{\pi}{4}\right), \tag{8}$$

with $\Delta k_0 = (\Delta k_{\max} - \Delta k_{\min})/2$ and $\Delta k_{\text{amp}} = \Delta k_{\max} - \Delta k_0$. Further, we decided to set back the exponent to the original value of 1/7 [*Brutsaert*, 1975] after evaluating fits of equation (3) to measured cloud-free emissivities at several radiation sites. Thus the apparent cloud-free emittance ϵ_{AC} in equation (3) is now formulated as

$$\epsilon_{\text{AC}} = \epsilon_{\text{AD}} + [k(t) + \Delta k(t)]\left(\frac{e}{T}\right)^{1/7}. \tag{9}$$

The modified CSI using equation (9) is called the cloud-free index (CFI):

$$CFI = \frac{\epsilon_{\text{A}}}{\epsilon_{\text{AC}}}. \tag{10}$$

Figure 1b shows how CFI can be used to separate cloud-free from overcast observations: CFI $\leq$ 1 normally indicates cloud-free conditions, and CFI > 1 indicates cloudy sky.

4.3. Determination of Site-Specific Functions $k(t)$ and $\Delta k(t)$

[16] In order to find $k(t)$ and $\Delta k(t)$ (equations (7) and (8)), single values of k are fitted at the diurnal and annual minimum and maximum of the periodical function $\gamma(t)$, i.e., afternoon (k_{day}) and early morning (k_{night}) for diurnal, and June–September (k_{summer}) and December–March (k_{winter}) for annual extrema in the Northern Hemisphere, and vice versa for the Southern Hemisphere. Hence four different values of k ($k_{\text{day,summer}}$, $k_{\text{night,summer}}$, $k_{\text{day,winter}}$, $k_{\text{night,winter}}$) and Δk ($\Delta k_{\text{day,summer}}$, $\Delta k_{\text{night,summer}}$, $\Delta k_{\text{day,winter}}$, $\Delta k_{\text{night,winter}}$) have to be fitted to measured cloud-free data to determine $k(t)$ and $\Delta k(t)$.

4.3.1. Annual Cycle of k and Δk

[17] We define the annual cycle (1 January to 31 December) of k for daytime (k_{day}) according to equation (7):

$$k_{\text{day}} = \overline{k}_{\text{day}} + k_{\text{day,amp}} \cos\left(\omega t - \frac{\pi}{4}\right), \tag{11}$$

with $\overline{k}_{\text{day}} = (k_{\text{day,summer}} + k_{\text{day,winter}})/2$ the annual average and $k_{\text{day,amp}} = k_{\text{day,winter}} - \overline{k}_{\text{day}}$ the annual amplitude of k for daytime and $\omega = 2\pi/P$ with period $P = 365$ days or $P = 366$ days. Analogously, we define the annual cycle of shift function Δk for daytime using equation (8):

$$\Delta k_{\text{day}} = \overline{\Delta k}_{\text{day}} + \Delta k_{\text{day,amp}} \cos\left(\omega t - \frac{\pi}{4}\right), \tag{12}$$

with $\overline{\Delta k}_{\text{day}} = (\Delta k_{\text{day,summer}} + \Delta k_{\text{day,winter}})/2$ the annual average and $\Delta k_{\text{day,amp}} = \Delta k_{\text{day,winter}} - \overline{\Delta k}_{\text{day}}$ the annual amplitude of Δk for daytime. The same definitions are used also for the annual cycles of k and Δk for nighttime (k_{night}).

4.3.2. Diurnal Cycle of k and Δk

[18] In order to calculate the diurnal cycle (0010 Local Time (LT) – 2400 LT) of $k = k(t)$, current values out of the annual cycles of k_{day} (equation (11)) and k_{night} on the actual day i were applied:

$$k(t) = \overline{k_i} + k_{\text{i,amp}} \cos\left(\omega t - \frac{\pi}{4}\right), \tag{13}$$

with $\overline{k_i} = (k_{i,\text{night}} + k_{i,\text{day}})/2$ the daily average and $k_{\text{i,amp}} = k_{i,\text{night}} - \overline{k_i}$ the daily amplitude of k, and $\omega = 2\pi/P$ with period $P = 144$ ten-minute values.

[19] The diurnal cycle (0010 LT–2400 LT) of Δk was calculated analogously:

$$\Delta k(t) = \overline{\Delta k_i} + \Delta k_{\text{i,amp}} \cos\left(\omega t - \frac{\pi}{4}\right), \tag{14}$$

with $\overline{\Delta k_i} = (\Delta k_{i,\text{night}} + \Delta k_{i,\text{day}})/2$ the daily average and $\Delta k_{\text{i,amp}} = \Delta k_{i,\text{night}} - \overline{\Delta k_i}$ the daily amplitude of Δk.

4.4. Example Fit of k and Δk

[20] We applied three successive years (1999–2001) to obtain the different k and Δk values for each radiation site except KWA, where CFI could be calculated only for the period 2000–2001. To fit $k_{\text{day,winter}}$ and $\Delta k_{\text{day,winter}}$ at WFJ, surface measurements of LDR, temperature, and humidity were used 3 hours ($\pi/4$) after the average Sun noontime at 1230 LT in Switzerland.

[21] In a first step, a first guess of 0.480 was chosen for $[k(t) + \Delta k(t)]$ in equation (9), and CFI was computed using equations (9), (2), and (10). Second, Stdev LDR was calculated over 2 hours (±1 hour) around 1530 LT (Stdev $\text{LDR}_{2\text{h}}$), and CFI was plotted for all situations with Stdev $\text{LDR}_{2\text{h}} \leq 1$ W m^{-2} shown in Figure 2. Overcast and cloud-free situations are clearly separated by different CFI values. Third, an upper CFI limit had to be chosen to exclude all overcast cases and outliers. Outliers are single points with at least 0.01 units distance to the next lower group of points (three and more points). Three outliers are indicated in Figure 2. For this example, an upper CFI limit of 0.99 was chosen to extract the cloud-free cases. From the remaining cases, the apparent cloud-free emissivities ϵ_{AC} were plotted against the ratio of water vapor pressure and absolute temperature (e/T) in Figure 3. Equation (9) with $\Delta k(t) = 0$ was fitted as y against e/T. The value $k_{\text{day,winter}} = 0.413$ was found for this case (Figure 3). Δk for a single fit is calculated using equation (9) and the emittance difference between y and

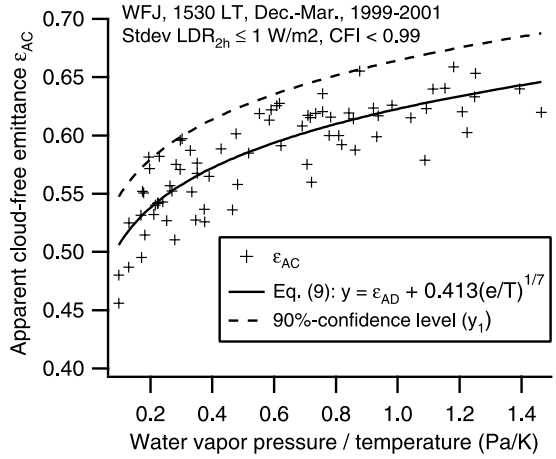

Figure 3. Apparent emittance of all cases in Figure 2 with CFI < 0.99 as a function of screen level water vapor pressure and temperature. The curve fit represents equation (9) with $\Delta k = 0$ and is used to determine k.

the upper 90% confidence level (y_1) of the function fit at the average value of $e/T = 0.80$ (Figure 3):

$$\Delta k = \frac{\epsilon_{AC,y_1} - \epsilon_{AC,y}}{(e/T)^{1/7}}. \quad (15)$$

$\Delta k_{day,winter} = 0.043$ was calculated for this case.

[22] A data set of at least 20 cloud-free cases is recommended to fit k and Δk for each season and time of day. Values of ϵ_{AD}, k, and Δk for all used radiation sites are given in Table 2.

4.5. Estimation of Partial Cloud Amount

[23] PCA in octas is estimated every 10 min using CFI and Stdev LDR, which is calculated over the last hour (60 min). A heuristic set of rules was developed to estimate PCA for about 2000 synoptic observations in Payerne for 1200 UTC (1300 LT) from 1996 to 2001. As an example, all cases between 0- and 2-octa PCA were plotted against Stdev LDR (e.g., Figure 1a), and increasing Stdev LDR limits were chosen to graphically separate 0-, 1-, and 2-octa PCA observations as well as possible. This procedure was repeated for all possible values of PCA (0–8 octas). In a second step, we introduced a new variable z using equation (10):

$$z = \mathrm{CFI}_{max} - \mathrm{CFI}_{cloud\text{-}free} \quad (16)$$

$$z = \frac{\epsilon_{overcast}}{\epsilon_{AC}} - \frac{\epsilon_{AC}}{\epsilon_{AC}} \quad (17)$$

with $\epsilon_{overcast} = 1$. Three CFI threshold limits, $1 + az$, $1 + bz$, and $1 + cz$, were further used to divide the whole range z into different sectors. A score index was applied to optimize the factors a, b, and c to get a maximum percentage of cases with minimized difference between estimated and observed PCA. The score index is defined as Score = 100 $[n_{(\pm 1 octa)}]/n$ (%), where $n_{(\pm 1 octa)}$ is the number of cases with maximum 1-octa difference between estimation and observation and n is the total number of cases. Score is defined analogously for a maximum 0- and 2-octa difference.

[24] The factors a, b, and c used for CFI threshold limits were optimized using the score index for a maximum 1-octa PCA difference. Values found specifically for Payerne are $a = 0.12$, $b = 0.21$, and $c = 0.38$, but further explorations showed that these values were applicable at all investigated sites. The set of heuristic rules with optimized factors a, b, and c is given in Table 3. The scheme using CFI, Stdev LDR, and the heuristic set of rules for estimating PCA is called automatic partial cloud amount detection algorithm (APCADA).

5. Results

5.1. Comparison of Partial Cloud Amount at ASRB Station Payerne

[25] Observed and APCADA-estimated partial cloud amounts (PCAs) were first compared in Payerne for the years 1996–1998 to have a data set independent from the CFI calibration period 1999–2001. Figure 4 shows different scores for maximum 0-, 1-, and 2-octa differences between estimated and observed PCAs. The average score for fully matched cases is 53.8% (45.4%–60.6%), and it is 87.2% (85.2%–88.6%) and 94.4% (93.8%–95.3%) for maximum 1- and 2-octa differences, respectively. Thus about 95% of all PCA estimations agree within ±2 octas with synoptic observations during daytime and nighttime.

Table 2. Station Short Name, Apparent Emittance ϵ_{AD} of Completely Dry Atmosphere, and Factors k and Δk Fitted for Cloud-Free Cases From 1999 to 2001[a]

		Summer (June–September)				Winter (December–March)			
		Day		Night		Day		Night	
Station	ϵ_{AD}	k	Δk	k	Δk	k	Δk	k	Δk
KWA	0.23	0.459	0.024	0.477	0.015	0.452	0.015	0.474	0.018
NYA	0.23	0.441	0.028	0.449	0.029	0.474	0.041	0.479	0.051
LOM	0.23	0.429	0.020	0.458	0.019	0.433	0.022	0.459	0.022
PAY	0.23	0.431	0.015	0.475	0.015	0.442	0.022	0.481	0.034
DAV	0.22	0.421	0.016	0.457	0.014	0.425	0.024	0.458	0.036
WFJ	0.21	0.412	0.017	0.428	0.027	0.413	0.043	0.425	0.042
JFJ	0.20	0.403	0.042	0.430	0.040	0.395	0.052	0.414	0.053

[a]KWA only 2000–2001.

Table 3. Scheme for Estimating Partial Cloud Amount Using Cloud-Free Index and Variability of Longwave Downward Radiation[a]

CFI (x)	Stdev LDR (y), W m^{-2}	PCA, octas
$x \leq 1$	$y \leq 0.5$	0
$x \leq 1$	$0.5 < y \leq 2$	1
$x \leq 1$	$y > 2$	2
$1 < x \leq (1 + az)$	$y \leq 1$	1
$1 < x \leq (1 + az)$	$1 < y \leq 2$	2
$1 < x \leq (1 + az)$	$y > 2$	3
$(1 + az) < x \leq (1 + bz)$	$y \leq 1$	2
$(1 + az) < x \leq (1 + bz)$	$y > 1$	4
$(1 + bz) < x \leq (1 + cz)$	$y \leq 4$	5
$(1 + bz) < x \leq (1 + cz)$	$y > 4$	6
$x > (1 + cz)$	$y > 8$	6
$x > (1 + cz)$	$2 < y \leq 8$	7
$x > (1 + cz)$	$y \leq 2$	8

[a]PCA, partial cloud amount; CFI, cloud-free index; Stdev LDR, variability of longwave downward radiation.

[26] Table 4 shows the percentage distribution of estimated and observed PCAs in Payerne for 1200 UTC from 1996 to 2002. Here, 47.6% of all observed or estimated cases are 7 or 8 octas (overcast), and 26.1% are 0 or 1 octas (cloud-free or almost cloud-free). Hence 26.3% of all observed cases show 2–6-octa PCA. The respective APCADA estimates vary strongly; for example, they range from 0 to 7 octas for 3-octa observed PCA. However, only 26 cases (1.1%) show a 4-or-more-octa difference between APCADA estimation and synoptic observation.

[27] Observed and APCADA-estimated PCAs are shown in Figure 5 for a single day in Payerne. The curve of APCADA estimates agrees well with synoptic observations of PCA. Four observations are fully matched, three have a 1-octa difference, and one observation shows a 2-octa difference.

5.2. Performance of APCADA in Different Climate Regimes

[28] APCADA was tested at radiation stations on different altitudes in the Alps and for one arctic and one tropical site. Table 5 gives the scores for a maximum 1-octa PCA difference between estimation and observation. All values are greater than 80%, except for KWA, where the minimum score is about 70%.

[29] Seasonal score rates are given in Table 6 for the ASRB station Locarno-Monti for 1200 UTC observations from 1996 to 2002. Lower scores for a maximum 0- or 1-octa PCA difference are found for springtime and summertime, but scores remain stable for a maximum 2-octa difference throughout the year.

6. Discussion

6.1. Limitations Comparing Synoptic and Estimated Partial Cloud Amount

[30] Various points complicate the comparison of observed and estimated partial cloud amount (PCA):

[31] 1. The relation between sky cover and measured LDR is disturbed through the synoptic rule that even a small cloud in an almost cloud-free sky leads to 1-octa cloud amount, even if the cloud-covered area is far less than 1 octa.

[32] 2. A major disadvantage of observations is the missing information about the hemispherical distribution of cloud amount. Clouds near zenith have a larger influence on LDR than clouds near the horizon because of shorter distance and larger radiant intensity, which is proportional to the cosine of the zenith angle. Therefore small amounts (up to 2 octas) of convective clouds bound to surrounding mountain chains have no detectable influence on LDR and are therefore missed by APCADA. For diurnal cycle, results in Figure 4 indicate that mainly the score for maximum 0-octa PCA difference is decreased in the early evening (1800 UTC) because of the rising number of convective clouds near the horizon and the previously mentioned rule for very small clouds. For the annual cycle, results in Table 6 show that the dominance of convective clouds in Switzerland in spring and summer slightly reduces the scores for a maximum 0- and 1-octa PCA difference, but the score for a maximum of 2 octas remains stable for all seasons.

[33] 3. Time of observation and observed cloud amounts for the same sky cover vary slightly for each synoptic observer. Hence observation and estimation of PCA can strongly disagree when observations are taken too early or too late.

[34] 4. Cirrostratus was observed for most of the outliers with a 4-or-more-octa PCA difference in the upper right

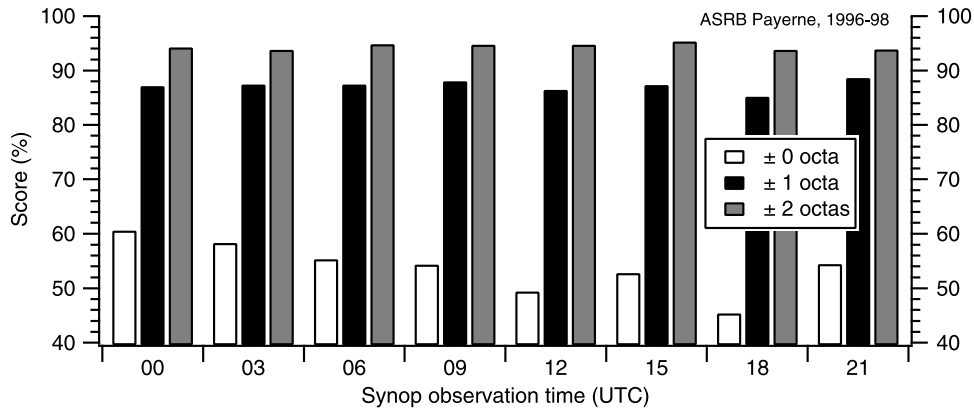

Figure 4. Diurnal cycle of score index for maximum 0-, 1- or 2-octa difference between estimated and observed partial cloud amount in Payerne from 1996 to 1998. The score for the 0-octa difference decreases from about 60% at midnight to 45% in the late afternoon. Score rates for a maximum 1- or 2-octa difference remain stable all over the day.

Table 4. Contingency Matrix of Observed and Estimated Partial Cloud Amount for Payerne Given in Octas[a]

		Estimated								
Observed	Percentage	0	1	2	3	4	5	6	7	8
0	8.2	67.4	24.1	3.7	1.6	0.5	2.2	0	0.5	0
1	17.9	61.3	28.3	7.9	1.7	0.3	0.5	0	0	0
2	7.4	20.3	40.1	24.0	9.6	3.0	1.2	1.2	0.6	0
3	5.2	9.4	18.8	27.3	20.5	12.0	2.6	6.0	3.4	0
4	4.3	0	13.1	23.2	25.3	15.2	4.0	14.2	4.0	1.0
5	3.3	0	2.7	10.8	12.2	12.2	13.5	24.3	20.3	4.0
6	6.1	0	0	2.9	8.6	10.8	7.2	38.1	23.0	9.4
7	17.4	0	0	0	1.0	1.5	2.8	14.4	45.1	35.2
8	30.2	0	0	0	0	0	1.3	1.0	19.5	78.2

[a]Percentage of observed partial cloud amount (PCA) for 2272 (=100%) cases at 1200 UTC (1300 LT) and percentage distribution of estimated PCA for each observed octa.

corner in Table 4, but the influence on LDR rather indicated a thin altostratus layer. The problem in distinguishing between middle and high clouds further intensifies during nighttime, when light conditions are poor. The percentage of outliers with cirrus clouds observed increases during nighttime compared to daytime in Payerne (not shown).

[35] Taking all points mentioned above into account, the overall agreement of estimated and observed PCAs is astonishingly good for all seasons (Table 6) and times of the day (Figure 4 and Table 5). Therefore the assumption of a periodic function for the vertical temperature gradient $\gamma(t)$ at the surface for the diurnal and annual cycle leads to good agreement between observed and estimated PCA at all tested radiation sites.

[36] The availability of APCADA-estimated PCA depends on the number of simultaneously available LDR, temperature, and humidity measurements. For the investigated ASRB data sets (Table 1), APCADA-estimated PCA was available for 98.9% of all possible 10-min values in Payerne, and still for 95.4% of all possible 10-min values at Jungfraujoch, where measurements are taken under harsh alpine weather conditions. At the BSRN station NYA, 99.0% of all possible PCA estimates were available, and 94.1% were available at KWA.

6.2. Comparison of Single Day in Payerne

[37] APCADA was designed for real-time processing of and monitoring of PCA. Figure 5 shows the comparison of observed and APCADA-estimated PCAs, which agree with less than a 1-octa difference on average. PCA is calculated from CFI and Stdev LDR according to the rules in Table 3. APCADA is suitable for detecting short-time occurrences of clouds between synoptic observations, e.g., at 1530 UTC. Thus the high temporal resolution of 10 min allows one to compare APCADA estimates with cloud cover measurements from other high temporal cloud detection systems at the Earth's surface and from satellite-based schemes.

6.3. Implementation of APCADA in Different Climate Zones

[38] APCADA has been adapted to five radiation stations in the Swiss Alps, one site in the Arctic sea on Spitzbergen, and one site in the tropical Pacific ocean. Locations of the different radiation sites in the Alps are distributed over a wide range of altitudes and therefore cover different climate zones with annual mean temperatures from 13° (LOM) to −7° Celsius (JFJ). Topography varies from site to site: LOM and DAV are situated in valleys, and WFJ and JFJ are crest stations with harsh weather conditions. PAY is located on a wide plateau, which is surrounded by the Alps to the south and the Jura mountains to the northwest. The winter half year (October–March) in Switzerland is predominantly characterized by stratiform clouds, whereas the summer half year (April–September) is dominated by convective clouds. Maritime influences dominate the climate at NYA and KWA. Results shown in Figure 4 and Table 5 show that APCADA was successfully adapted to radiation sites in various climate zones from low to high latitudes. The lowest score rates are

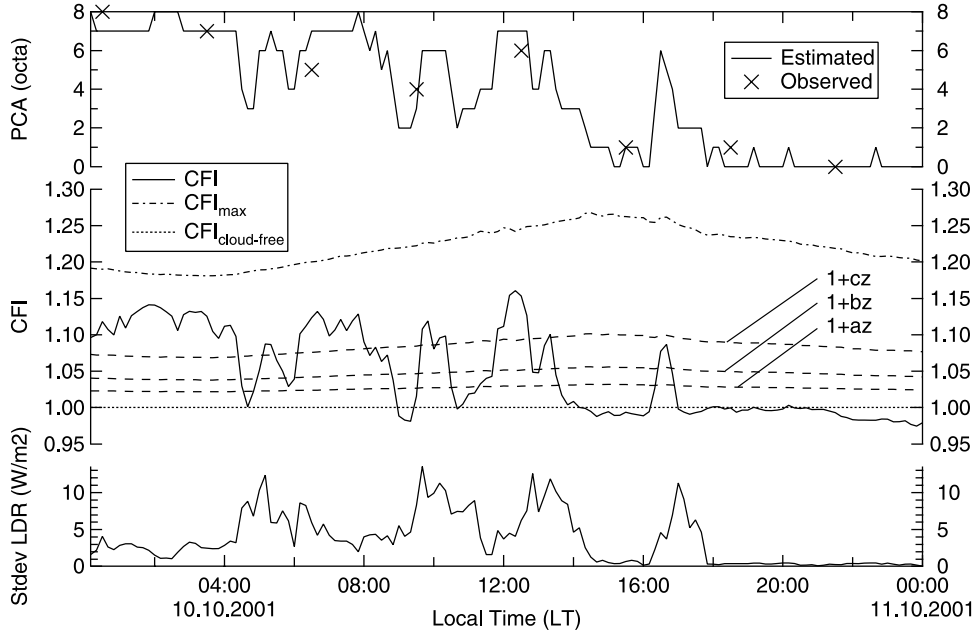

Figure 5. Comparison of observed and estimated partial cloud amount for a single day in Payerne.

Table 5. Diurnal Cycle and Daily Averages of Scores for Maximum 1-Octa Difference Between Estimated and Observed Partial Cloud Amount

LT	PAY	LOM	JFJ	DAV	WFJ	NYA	KWA[a]
0100	86.6	...	...	...	...	...	83.3
0400	86.7	...	...	...	...	...	...
0700	87.0	88.1	84.2	92.0	87.2	83.2	76.2
1000	88.0	87.6	84.7	...	...	...	...
1300	86.9	85.5	82.2	87.6	89.4	82.0	77.7
1600	88.0	85.7	82.9	...	...	...	...
1900	84.3	87.3	80.6	84.9	83.8	83.0	69.6
2200	87.3	...	...	...	...	...	...
Average	86.9	86.8	82.9	88.2	86.8	82.7	76.7

[a]LT minus 1 hour.

found for KWA (Table 5). Investigations showed that the percentage of broken PCA (2–6 octas) in KWA is over 60% compared to about 30% in PAY, which decreases the precision of APCADA. The diurnal cycle of the amount of convective clouds in KWA is also reflected in the according score rates: The minimum is reached in late afternoon, and the maximum is reached at midnight.

6.4. Total Cloud Amount Detection Without High Clouds

[39] APCADA is able to detect only clouds that have a measurable effect on LDR, i.e., increasing LDR variability and/or additional effect on LDR at the Earth's surface. Hence the comparison of estimated and observed sky cloud cover had to be restricted to the total amount of clouds without high clouds. Concerning daily weather forecast, information about cloud amount affecting sunshine duration, i.e., low and middle clouds, is of interest for a broad general public. However, further investigations are needed to combine APCADA with other cloud detection systems during daytime and nighttime to include the occurrence of high clouds for climatological studies.

7. Conclusions

[40] An enhanced version of the clear-sky index (CSI), called the cloud-free index (CFI), was formulated to reduce the inadvertent diurnal and annual cycle of CSI for cloud-free cases. CFI is calculated from measurements of longwave downward radiation (LDR), temperature, and relative humidity at screen level height. A real-time processing system, called the automatic partial cloud detection algorithm (APCADA), has been developed to automatically estimate partial cloud amount (PCA) every 10 min during daytime and nighttime on the basis of CFI and the variability of LDR.

[41] APCADA-estimated PCAs were compared with synoptic observations from five radiation sites at different altitudes in the Swiss Alps, from one site in an arctic climate, and from one location with a tropical climate. In about 82–87% of all cases the maximum cloud amount difference between estimate and observation was smaller or equal to 1 octa both during daytime and nighttime for high-latitude and midlatitude sites. At the tropical site Kwajalein the corresponding scores range from 70% to 83% because of dominance of convective clouds with predominantly 2–6-octa sky cloud cover. Average site percentages for maximum ±2-octa cloud amount difference range from 90% up to 95% for all investigated radiation stations.

[42] The implementation of APCADA at a radiation site is independent from the knowledge of synoptic cloud cover observations. Thus the existing LDR series of measurements with accompanying temperature and humidity measurements are suitable for postprocessing by APCADA to investigate the long-term behavior of cloud amount with high temporal resolution. APCADA estimates of PCA were available for from 94% (KWA) up to 99% (PAY) of all possible 10-min data depending on the simultaneous availability of LDR, temperature, and relative humidity measurements at screen level height.

Table 6. Annual Cycle of Scores for Maximum 0-, 1-, or 2-Octa Difference Between Estimated and Observed Partial Cloud Amount in Locarno-Monti for 1200 UTC (1300 LT)

	Score, %			
Season	±0	±1	±2	N
Winter (Jan.–March)	54.9	87.8	95.2	559
Spring (April–June)	38.9	83.4	95.8	499
Summer (July–Sept.)	34.6	82.8	95.1	512
Autumn (Oct.–Dec.)	55.9	87.2	94.7	564

[43] **Acknowledgments.** This investigation was financed by the Swiss National Science Foundation under grant 21-58746.99 and supported by the Institute of Atmospheric and Climate Science of ETH-Zürich. The authors wish to thank MeteoSwiss for providing meteorological data and technical support for the ASRB network.

References

Aviolat, F., T. Cornu, and D. Cattani (1998), Automatic clouds observation improved by an artificial neural network, *J. Atmos. Oceanic Technol.*, *15*, 114–126.

Beaubien, M., and A. Bisberg (1999), A new CCD-based instrument for the automatic determination of cloud cover, paper presented at 10th Atmospheric Radiation Conference, Am. Meteorol. Soc., Madison, Wisc.

Berk, A., G. P. Anderson, P. K. Acharya, J. H. Chetwynd, L. S. Bernstein, E. P. Shettle, and M. W. Matthew (2000), MODTRAN4 users manual, Air Force Res. Lab., Hanscom Air Force Base, Mass.

Brutsaert, W. (1975), On a derivable formula for longwave radiation from clear sky, *Water Resour. Res.*, *11*(3), 742–744.

Buck, A. L. (1981), New equation for computing water vapour pressure and enhancement factor, *J. Appl. Meteorol.*, *20*, 1527–1532.

Feister, U., J. Shields, M. Karr, R. Johnson, K. Dehne, and M. Woldt (2000), Ground-based cloud images and sky radiances in the visible and near infrared region from whole sky imager measurements, paper presented at Climate Monitoring: Satellite Application Facility Training Workshop, Dtsch. Wetterdienst, Dresden.

Gillotay, D., T. Besnard, and F. Zanghi (2002), A systematic approach of the cloud cover by thermic infrared measurements, paper presented at 18th Conference on Weather Analysis and Forecasting, Am. Meteorol. Soc., Fort Lauderdale, Fla.

Hahn, C. J., S. G. Warren, and J. London (1995), The effect of moonlight on observation of cloud cover at night, and application of cloud climatology, *J. Clim.*, *8*(5), 1429–1446.

Long, C. N., and T. P. Ackermann (2000), Identification of clear skies from broadband pyranometer measurements and calculation of downwelling shortwave cloud effects, *J. Geophys. Res.*, *105*, 15,609–15,626.

Long, C. N., and J. DeLuisi (1998), Development of an automated hemispheric sky imager for cloud fraction retrievals, paper presented at 10th Symposium on Meteorological Observations and Instrumentation, Am. Meteorol. Soc., Phoenix, Ariz.

Marty, C. (2000), Surface radiation, cloud forcing and greenhouse effect in the Alps, Ph.D. thesis, Inst. of Clim. Res., ETH Zürich.

Marty, C., and R. Philipona (2000), The clear-sky index to separate clear-sky from cloudy-sky situations in climate research, *Geophys. Res. Lett.*, *27*, 2649–2652.

Marty, C., R. Philipona, C. Fröhlich, and A. Ohmura (2002), Altitude dependence of surface radiation fluxes and cloud forcing in the Alps: Results from the alpine surface budget network, *Theor. Appl. Climatol.*, *72*, 137–155.

Nadolski, V. (1995), United States moves ahead with deployment of the automated surface observing system, *ICAO J.*, *50*(8), 10–11.

Ohmura, A. (2001), Physical basis for the temperature-based melt-index method, *J. Appl. Meteorol.*, *40*, 753–761.

Ohmura, A., et al. (1998), Baseline surface radiation network (BSRN/WCRP): New precision radiometry for climate research, *Bull. Am. Meteorol. Soc.*, *79*, 2115–2136.

Philipona, R., C. Fröhlich, and C. Betz (1995), Characterization of pyrgeometers and the accuracy of atmospheric long-wave radiation measurements, *Appl. Opt.*, *34*, 1598–1605.

Philipona, R., C. Marty, C. Fröhlich, and A. Heimo (1996), Measurements of the longwave radiation budget in the Alps, in *IRS 96: Current Problems in Atmospheric Radiation*, edited by W. L. Smith and K. Stamnes, pp. 786–789, A. Deepak, Hampton, Va.

Philipona, R., et al. (1998), The baseline surface radiation network pyrgeometer round-robin calibration experiment, *J. Atmos. Oceanic Technol.*, *15*, 687–696.

Philipona, R., et al. (2001), Atmospheric longwave irradiance uncertainty: Pyrgeometers compared to an absolute sky-scanning radiometer, AERI and radiative transfer model calculations, *J. Geophys. Res.*, *106*, 28,129–28,141.

Ruppert, P. (1991), THYGAN, Beschreibung der Funktion und der Technik, *Tech. Rep. 164*, Fed. Off. of Meteorol. and Climatol., Zürich.

B. Dürr and R. Philipona, Physikalisch-Meteorologisches Observatorium Davos, World Radiation Center, PMOD/WRC, Dorfstrasse 33, CH-7260 Davos-Dorf, Switzerland. (b.duerr@pmodwrc.ch; r.philipona@pmodwrc.ch)